POTSDAM-INSTITUT FÜR KLIMAFOLGENFORSCHUNG

Originally published as:

Su, B., Huang, J., Fischer, T., Wang, Y., Kundzewicz, Z. W., Zhai, J., Sun, H., Wang, A., Zeng, X., Wang, G., Tao, H., Gemmer, M., Li, X., Jiang, T. (2018): Drought losses in China might double between the 1.5 °C and 2.0 °C warming. - Proceedings of the National Academy of Sciences of the United States of America (PNAS), 115, 42, 10600-10605

DOI: 10.1073/pnas.1802129115

Drought losses in China might double between the 1.5 °C and 2.0 °C warming

Buda Su[a,b,c,1], Jinlong Huang[a,d,1], Thomas Fischer[c,e], Yanjun Wang[b], Zbigniew W. Kundzewicz[f,g,2], Jianqing Zhai[b,c], Hemin Sun[b], Anqian Wang[a,d], Xiaofan Zeng[h], Guojie Wang[b], Hui Tao[a], Marco Gemmer[c,e], Xiucang Li[b,c], and Tong Jiang[b,c,2]

[a]State Key Laboratory of Desert and Oasis Ecology, Xinjiang Institute of Ecology and Geography, Chinese Academy of Sciences, Urumqi 830011, China; [b]Collaborative Innovation Center on Forecast and Evaluation of Meteorological Disaster, School of Geographic Sciences, Nanjing University of Information Science & Technology, Nanjing 210044, China; [c]National Climate Center, China Meteorological Administration, Beijing 100081, China; [d]University of Chinese Academy of Sciences, Beijing 100049, China; [e]Department of Geosciences, Eberhard Karls University, 72074 Tübingen, Germany; [f]Institute for Agricultural and Forest Environment, Polish Academy of Sciences, 60809 Poznan, Poland; [g]Potsdam Institute for Climate Impact Research, 14473 Potsdam, Germany; and [h]School of Hydropower & Information Engineering, Huazhong University of Science and Technology, Wuhan 430074, China

Edited by Amir AghaKouchak, University of California, Irvine, CA, and accepted by Editorial Board Member Gregory P. Asner August 16, 2018 (received for review February 8, 2018)

We project drought losses in China under global temperature increase of 1.5 °C and 2.0 °C, based on the Standardized Precipitation Evapotranspiration Index (SPEI) and the Palmer Drought Severity Index (PDSI), a cluster analysis method, and "intensity-loss rate" function. In contrast to earlier studies, to project the drought losses, we predict the regional gross domestic product under shared socioeconomic pathways instead of using a static socioeconomic scenario. We identify increasing precipitation and evapotranspiration pattern for the 1.5 °C and 2.0 °C global warming above the preindustrial at 2020–2039 and 2040–2059, respectively. With increasing drought intensity and areal coverage across China, drought losses will soar. The estimated loss in a sustainable development pathway at the 1.5 °C warming level increases 10-fold in comparison with the reference period 1986–2005 and nearly threefold relative to the interval 2006–2015. However, limiting the temperature increase to 1.5 °C can reduce the annual drought losses in China by several tens of billions of US dollars, compared with the 2.0 °C warming.

drought | drought losses | projections | global warming | China

Droughts are major weather-driven natural disasters that encompass large areas. Droughts can occur everywhere, including water-rich areas, due to occasional anomalies in climatic variables. The impacts of drought events with similar intensity and duration can largely vary, depending on socioeconomic and environmental characteristics of the affected regions. Around the world, drought losses have significantly increased in recent years, for a range of reasons, including nonclimatic factors (1, 2). Enhanced drying has been observed and projected over many land areas under warming climate, due to increasing atmospheric concentrations of greenhouse gases (3–5). The direction of observed increase in global aridity is consistent with model-based projections (3). Since 2010, frequent and severe drought events in southern China, a region considered to be humid, have been given much attention and have resulted in national enhancement of drought research. Previous studies reported that significant dryness trends detected in the transitional belt of humid and arid climate regions in China for the last half-century and the reduction in regional precipitation play a major role in a changing pattern of drought intensity and duration (6–8).

With expected increases in severe and widespread drought events in the 21st century (3, 9) and further strong growth in the gross domestic product (GDP), more assets will be exposed to the impacts of droughts, which will eventually lead to higher drought losses in the future. To reduce the risk and impacts of a warming climate, the Paris Agreement proposes to hold the increase in global mean temperature to well below 2.0 °C above preindustrial levels and to pursue efforts to limit the warming to 1.5 °C (10). Most projections agree that the warming rate of China will be faster than the global mean (11) and the country might be seriously threatened by global warming-induced disasters. Existing studies in China focus mainly on projections of drought characteristics, with the estimation of drought losses being largely determined by changes in the physical drought parameters. To date, the inclusion of different shared socioeconomic pathways (SSPs; ref. 12) into a multiscenario approach of loss estimation has not been applied for drought projections over China. Hence, in our study, we project future drought losses in China by applying an approach consisting of multimodel scenario-comparison analyses and event-based loss estimation using two drought indices, namely the Standardized Precipitation Evapotranspiration Index (SPEI) and the Palmer Drought Severity Index (PDSI).

Projected Changes in Dryness Patterns

In this study, future characteristics of climate change impacts are analyzed using 22 ensemble runs from 13 global climate models (GCMs) in CMIP5 (Coupled Model Intercomparison Project phase 5): GFDL-ESM2M, HadGEM2-ES, IPSL-CM5A-LR, MIROC-ESM-CHEM, NorESM1-M, CNRM-CM5, CanESM2,

Significance

We project drought losses in China under global warming of 1.5 °C and 2.0 °C. To assess future drought losses, we project the regional gross domestic product under shared socioeconomic pathways instead of using a static socioeconomic scenario. We identify increasing precipitation and evapotranspiration patterns. With increasing drought intensity and areal coverage across China, drought losses will increase considerably. The estimated losses in a sustainable development pathway at 1.5 °C warming will be 10 times higher than in the reference period 1986–2005 and three times higher than in 2006–2015. Yet, climate change mitigation, limiting the temperature increase to 1.5 °C, can considerably reduce the annual drought losses in China, compared with 2.0 °C warming.

Author contributions: Z.W.K. and T.J. designed research; B.S., J.H., X.Z., and H.T. performed research; B.S., J.H., Y.W., J.Z., H.S., A.W., G.W., and X.L. analyzed data; and B.S., J.H., T.F., Y.W., Z.W.K., J.Z., H.S., A.W., X.Z., G.W., H.T., M.G., X.L., and T.J. wrote the paper.

The authors declare no conflict of interest.

This article is a PNAS Direct Submission. A.A. is a guest editor invited by the Editorial Board.

[1]B.S. and J.H. contributed equally to this work.

[2]To whom correspondence may be addressed. Email: kundzewicz@yahoo.com or jiangtong@cma.gov.cn.

This article contains supporting information online at www.pnas.org/lookup/suppl/doi:10.1073/pnas.1802129115/-/DCSupplemental.

GFDL-CM3, GFDL-ESM2G, IPSL-CM5A-MR, MIROC-ESM, MIROC5, and MRI-CGCM3. Two representative concentration pathways (RCPs) are considered, i.e., RCP2.6 and RCP4.5, which are the most appropriate scenarios for the Paris Agreement's target of keeping the global warming below 1.5 °C or 2.0 °C compared with preindustrial times. Global surface mean temperature in 1986–2005 was 0.61 °C warmer than the preindustrial levels (11), and further increase of 0.89 °C or 1.39 °C, respectively, indicates global warming by 1.5 °C or 2.0 °C. Using a multimodel median, projections for 20-y intervals were estimated when the average global warming reaches the 1.5 °C and 2.0 °C thresholds, respectively, under RCP2.6 and RCP4.5. It is estimated that the 1.5 °C warming threshold would be reached in 2020–2039 under RCP2.6 and the 2.0 °C in 2040–2059 under RCP4.5 (13).

The models project tendencies of precipitation increase for both the 1.5 °C and 2.0 °C global warming levels in the whole of China, with higher model agreement at the northern regions (Fig. 1 *A* and *E*). The increasing trend is agreed by more than 66% of GCM runs for 80% and 96% of grids over China at the 1.5 °C and 2.0 °C warming, respectively. Considerably more significant precipitation increases are projected for the period 2040–2059, demonstrating a positive correlation between precipitation and temperature for the next decades.

Significant increases in potential evapotranspiration are projected throughout China for both target periods (Fig. 1 *B* and *F*). The positive changes in evapotranspiration are more significant for the 2.0 °C warming period of 2040–2059, in the parts of North, Northwest, and Southwest China than those at the 1.5 °C warming. Compared with precipitation, evapotranspiration increase is more obvious in southern China as a whole. The increasing trend is consistent for most GCM runs for 85% and 98% of grid cells over China at the 1.5 °C and 2.0 °C warming scenarios, respectively.

Drought conditions can be assessed from different meteorological, hydrological, and socioeconomic aspects, so that decision on the choice of drought indices is needed (14–16). A simple and commonly used index, the Standardized Precipitation Index (SPI), allows the direct comparison of precipitation anomalies among different climatic regions. Nevertheless, it is widely acknowledged that evapotranspiration plays a major role in the generation of droughts in the warmer world (4, 17). Hence, two other drought indices are used to address the long-term characteristics of dryness and wetness in current study. The SPEI (cf. refs. 18 and 19) takes precipitation, temperature, and evapotranspiration into account and thus represents a simple climatic water balance. The PDSI (cf. refs. 20 and 21) takes precipitation, evapotranspiration, and available water storage capacity as input to compute a water balance for area of interest.

With regard to the reference period, dryness in most of southern China is identified consistently by both the SPEI and the PDSI indices in the warming climate. According to SPEI, large areas in Northeast and North, some parts of East, Central, and Southwest China might be in wetter conditions, but vast areas of western and southern China will be drier at the 1.5 °C warming level. Percentages of area getting wetter and drier will be about 39% and 61%, and the changes are significant at 7% and 36% of the entire territory of China. Nearly 75% of the area of China will be getting drier and, for 51% of the area, change is projected to be significant at the 2.0 °C, whereas wetter conditions will be in Northeast, small fractions of North, Northwest, Southwest, and East China (Fig. 1 *C* and *G*). A comparatively weaker drying trend is estimated by PDSI, which shows significant wetness in large parts of northern China, except for parts of Northwest and Northeast regions. Meanwhile, at least 66% of GCMs at both the 1.5 °C and 2.0 °C warming agree on significant increase of dryness conditions projected by PDSI in southern China. About 40% and 37% of the country area are projected to

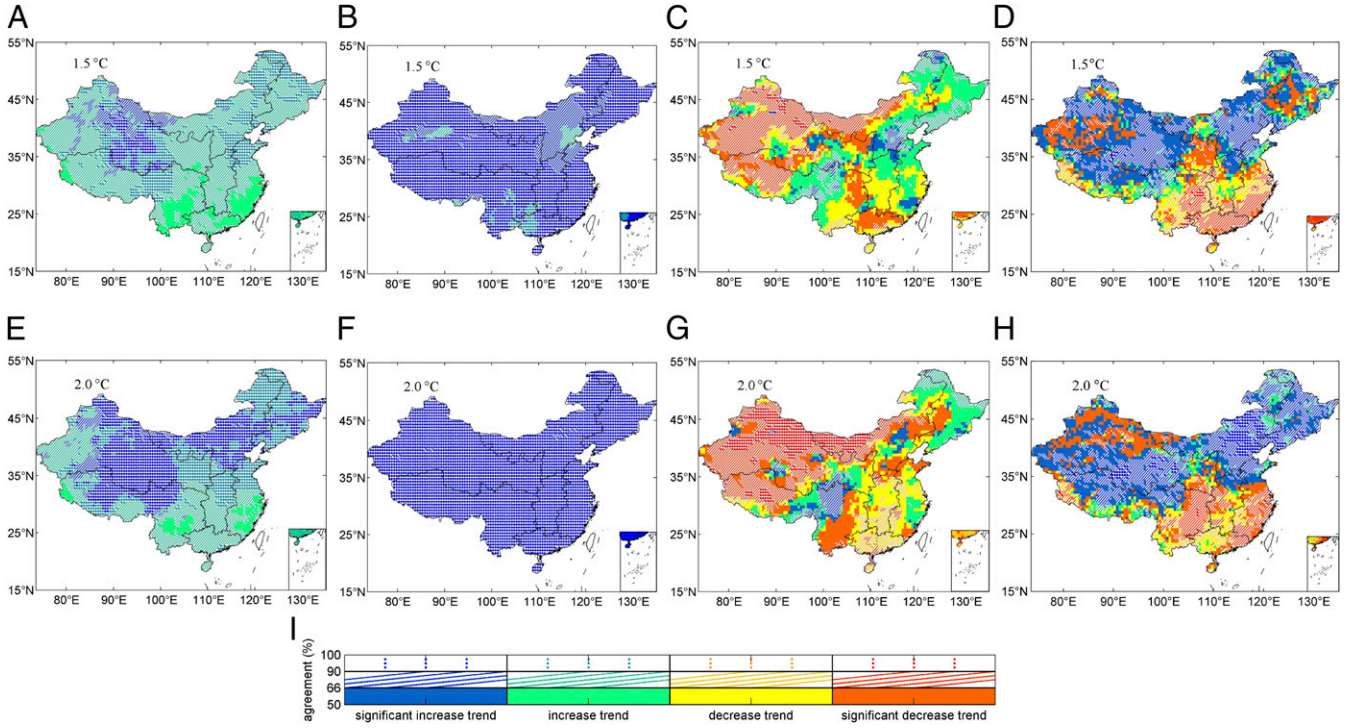

Fig. 1. Projected changes in precipitation (*A* and *E*), potential evapotranspiration (*B* and *F*), drought conditions of the SPEI (*C* and *G*), and the PDSI (*D* and *H*) by multimodel median for the 1.5 °C and 2.0 °C warming scenarios (corresponding to periods of 2020–2039 and 2040–2059, respectively) relative to the reference period (1986–2005) over China. The significance of the changes was tested with the two-sample *t* test at the 0.05 significance level. The similarity among the 22 GCM runs is given for the 90∼100% and 66∼90% (*I*) agreement level. Polygons denote subregions (defined in *SI Appendix*, Fig. S1) in China.

get drier, with a significant decrease at 25% and 27% of the area for the 1.5 °C and the 2.0 °C, respectively (Fig. 1 *D* and *H*).

Projection of Droughts

A spatial-temporal drought event is usually characterized by its duration, intensity, and contiguous areal coverage (8, 22, 23). In this study, we define a drought event as occurring if the SPEI ≤ −1 (or the PDSI ≤ −2) at the area exceeding 50,000 km^2 (*SI Appendix*, Table S4), because events with such thresholds usually lead to considerable economic losses (24).

For the period of 1986–2005, average intensities of GCM-simulated drought events over China as deduced by the SPEI and PDSI fluctuate around −1.83 and −3.6, respectively, indicating severe dryness. Higher intensities are projected with the climate warming. The average drought intensity, determined by the SPEI, will further increase to −2.10 and −2.25 at the 1.5 °C and the 2.0 °C warming level, respectively, and that by the PDSI, will reach −4.0 and −4.2, indicating extremely dry conditions. Large-area droughts with more than 2 million km^2 coverage are projected to have slightly lower average intensities than small-area droughts (Fig. 2 *A* and *C*).

Along with intensities, contiguous area of drought events for both warming levels will also increase. The average drought event area for the SPEI index criterion is ∼608,300 km^2 for the reference period, projected to increase to 709,400 km^2 and 880,800 km^2 for the 1.5 °C and the 2.0 °C warming, respectively, i.e., an increase of 16.6% and 44.8%. Meanwhile, increase in average drought coverage from 475,900 km^2 for the reference period to 486,500 km^2 and 518,200 km^2 by a rate of 2.2% and 8.9% is estimated for the PDSI index, for the 1.5 °C and the 2.0 °C level, respectively (Fig. 2 *B* and *E*).

In contrast, total frequency of drought events is projected to increase slightly for both the 1.5 °C and 2.0 °C warming scenarios, compared with the reference period. Small-area droughts are projected to decrease in frequency, but larger drought events with an area greater than 500,000 km^2 will likely occur more frequently for the SPEI index. However, for the PDSI index, frequencies of drought events with different coverage are all projected to increase (Fig. 2 *C* and *F*).

Spatially, as indicated by SPEI, drought frequency for the 1.5 °C warming level is projected to decrease slightly in Northeast and Central China. The decreasing trend extends into the 2.0 °C warming level in the Northeast region, while drought frequency increases in most other regions. As for the contiguous drought area, all regions show persistent increasing trends in the future, with the strongest increase in Northwest China, followed by North, Northeast, and South China. Drought intensities also increase consistently in all regions until 2040–2059, while a stronger increase is projected in Northwest, North, East, and Southwest China. According to the PDSI, regions with increased drought frequency are mainly found in Northeast, East, and Southwest China, and increased drought areas are projected to occur in East, South, and Northwest China in the warming climate. To sum up, it was projected that droughts would be more intense throughout China with increased occurrence in East and Southwest regions and larger areal coverage in East, South, and Northwest regions under the warming scenarios, relative to the reference period for both the SPEI and PDSI, but drought severity is projected to be greater for SPEI (Fig. 3).

Event-Based Estimation of Drought Losses

Assumption of a fixed population or an economic status for a historical period is usually made to study the future impacts of a changing climate (25). However, an adequate assessment of climate change impacts must take future socioeconomic development into account, as the economy and the population will be exposed to increasing risk of climate disasters. To this end, five shared socioeconomic pathways (SSPs) have been projected to represent different climate change strategies for mitigation and adaptation. The SSPs include a sustainable world (SSP1), a pathway of continuing historical trends (SSP2), a strongly fragmented world (SSP3), a highly unequal world (SSP4), and a growth-oriented world (SSP5) (26). Among combinations of different greenhouse gas concentration trajectories and socioeconomic pathways, some SSP-RCP combinations are unlikely to occur, e.g., SSP3-RCP2.6 and SSP1-RCP8.5 (27). Considering the socioeconomic challenges to mitigation by different development roads, the RCP2.6 scenario is associated with SSP1 and SSP4, while the RCP4.5 scenario is associated with the other three SSPs (SSP2, SSP3, SSP5).

For the reference period of 1986–2005, average annual drought losses in China amounted to about 4.2 billion US dollars (USD), or 0.23% of the national GDP (*SI Appendix*, Table S6). With the accelerated increase of GDP and improved adaptation capacity,

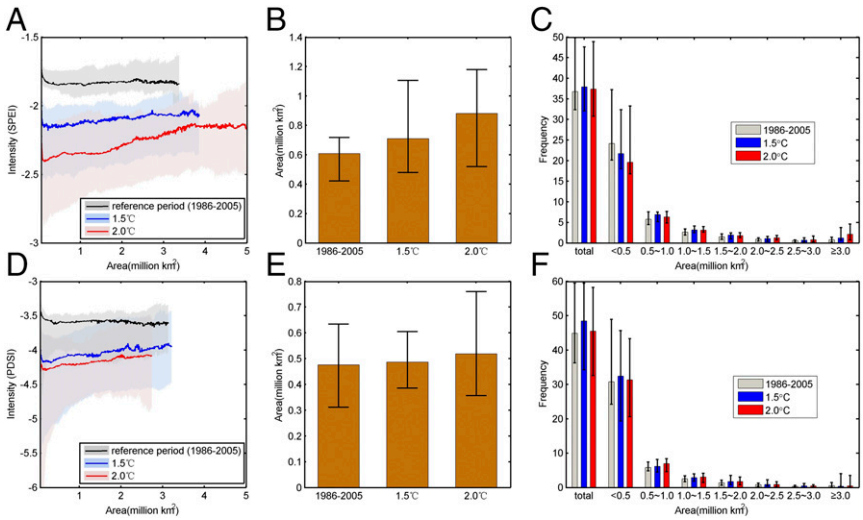

Fig. 2. Averaged drought intensity at different contiguous drought areas (*A* and *D*), averaged coverage of drought events (*B* and *E*), and annual frequency of drought events with different coverage (*C* and *F*) in China for the 1.5 °C and 2.0 °C global warming period and the reference period (1986–2005). Drought characteristics in *A*–*C* and *D*–*F* are deduced by the SPEI and PDSI, respectively. Shadows and lines in *A* and *D* are the bands and median, respectively, for 22 GCM runs. Histograms and black vertical lines in *B* and *C* and *E* and *F* denote the median and range of multimodel projections, respectively.

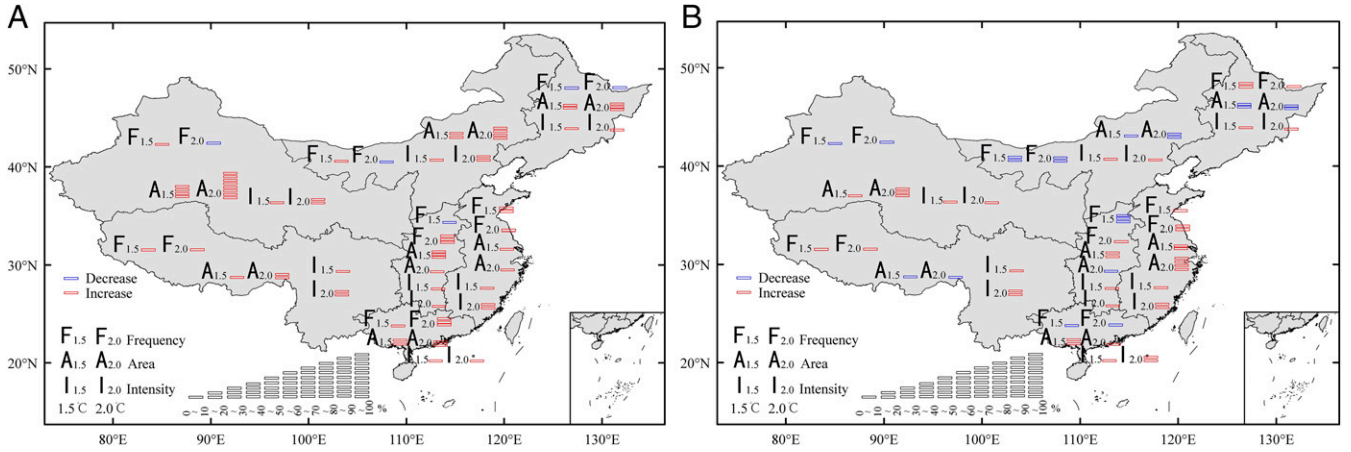

Fig. 3. Percentage change of annual frequency, areal coverage, and intensity of drought events resulting from multimodel median for two levels of global warming (1.5 °C and 2.0 °C), in comparison with the reference period (1986–2005) in seven subregions in China as indicated by the SPEI (*A*) and the PDSI (*B*), respectively.

the share of drought losses to GDP decreased to 0.16% in 2006–2015 with a minimum of 0.04% in 2012 (24). Future drought losses are assessed based on the projected drought intensity by the GCM simulations, the estimated socioeconomic exposure under SSPs, and the "intensity-loss rate" curve changing with time. For setting up intensity-loss rate curve, the relationship between the percent of annual recorded direct economic losses on GDP exposed to drought events and the historical annual average intensity of drought events was established first, and was developed further, to reflect improvements in adaptation capacity in the future (*SI Appendix*, Figs. S8–S10).

Multimodel scenario-comparison analyses show that projected drought losses in a warming climate in China will be higher than those in the reference period, 1986–2005, and in the more recent interval, 2006–2015, with 44 combined results from the 22 GCMs and the two drought indices showing the same direction of change (Fig. 4*A*). A strong agreement from at least 30 results of 44 combinations for all SSPs indicate exceeding of the share of drought losses on GDP in the warming scenarios than that of the current status with higher probability (Fig. 4*B*).

In a sustainable world with effective mitigation and adaptation (SSP1) and with the global warming limited to 1.5 °C, drought-induced economic losses might reach ∼47 billion USD per year by median of 44 estimations from 22 GCM runs and two drought indices, with 95% confidence interval of 44–55 billion (Fig. 4*A*). This projected annual loss is about 10 times higher than for the reference period, while the increase in population and exposed economic assets is included. Taking this into account, the relation of losses to the projected national GDP seems useful. Accordingly, the projected annual average loss for a sustainable world (SSP1) at 1.5 °C warming is about 0.19% of the projected national GDP, lower than that for the reference period of 1986–2005 (Fig. 4*B*). In a highly unequal world of SSP4, not much difference is projected for GDP development in China before the mid-21st century (*SI Appendix*, Fig. S7), estimated annual drought loss will only be slightly lower than for a sustainable world with absolute value of 46 [95% confidence interval: 43–54] billion USD (Fig. 4).

Based on a continuation of the historical trend pathway SSP2 and limiting the global warming to 2.0 °C scenario, the estimated annual drought loss will increase to 75 [95% confidence interval: 68–84] billion USD, which amounts to 0.21% of the projected national GDP of the corresponding period. In a strongly fragmented world SSP3 and the 2.0 °C target, drought loss will be about 61 [95% confidence interval: 56–68] billion USD, accounting for ∼0.21% of the GDP. In a growth-oriented world

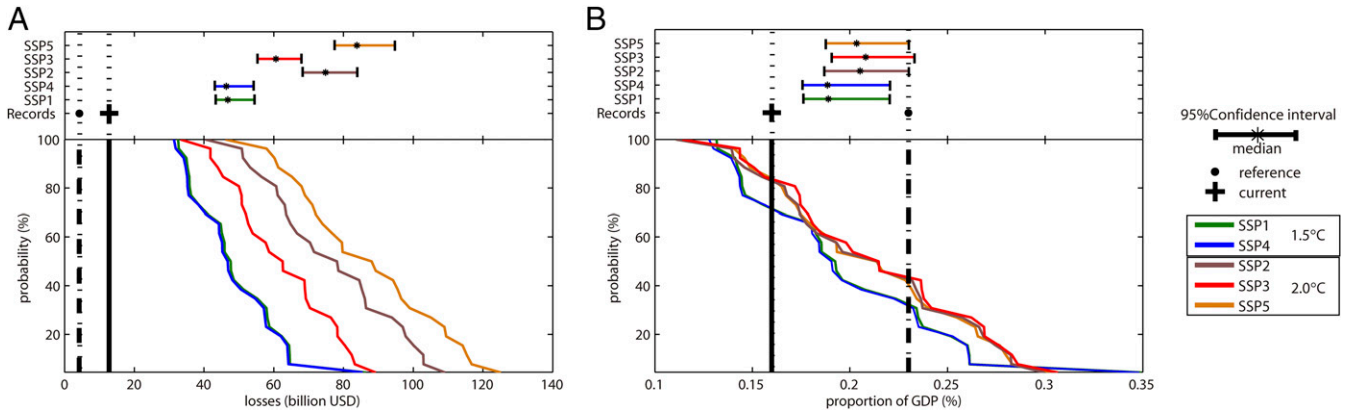

Fig. 4. Drought losses (*A*) and their share of GDP (*B*) at the global warming 1.5 °C and 2.0 °C levels under SSPs in China. Probability in vertical axis represents percentage of results exceeding a given loss (*A*) or given loss' share of GDP (*B*) of 44 combinations of 22 GCMs and two drought indices. Dotted black lines denote the recorded annual mean losses and their share of GDP in reference period and current status. Confidence intervals (95%) of projected losses and their share of GDP are shown for different SSPs. Asterisk is the multimodel median.

SSP5 of 2.0 °C, average drought loss is estimated to reach about 84 [95% confidence interval: 77–95] billion USD per year. This high figure reflects only 0.20% of the projected national GDP, due to the strong increase in the projected national GDP within SSP5. The annual average drought loss for the 2.0 °C warming level under the SSP5 is estimated to be 20 times of that in the reference period 1986–2005 and 1.8 times of that in the 1.5 °C warming level under SSP1 or SSP4, respectively (Fig. 4).

With increasing drought hazards and expected economic development across China, drought losses are projected to reach more than 80 billion USD, being higher by more than 30 billion USD in the 2.0 °C warming scenario under the growth-oriented world of SSP5 compared with that of 47 billion in the 1.5 °C warming scenario under the SSP1. Annual growth of GDP under pathways SSP1 and SSP5 are projected to be around 773 and 656 billion USD, respectively (*SI Appendix*, Fig. S7). That is, nearly 6.1% of the increase of GDP per year in the 1.5 °C warming world might be offset by drought losses, and the percent will increase to 12.8% in the 2.0 °C warming world.

Discussion and Conclusions

To evaluate climatic drought, many indices have been developed to describe variation of dry and wet episodes. The SPEI is designed to compare the evaporative demand by the atmosphere with the water availability, while the PDSI tried to represent the true water balance of the soils (19). Findings from the PDSI in our study are in line with regional results from a global-scale study by Sheffield et al. (28), who applied PDSI_PM that takes into account changes in available energy, humidity, and wind speed as we did in our study, and results from Wang et al. (29), who applied soil moisture condition as an indicator. Since PDSI depends on the current water availability, drought conditions assessed by the PDSI are less severe than the SPEI. Droughts in 1984–2015 in China, characterized by the PDSI, show a nonsignificant aggravation trend, but a significant dryness trend is detected by the SPEI (*SI Appendix*, Fig. S5). Especially in arid and semiarid climate regions, where annual precipitation is below 400 mm with a vast of area even less than 200 mm, a dryness trend is detected by the SPEI, but a weak wetting trend is found when the PDSI is examined. Note that the correlation between the PDSI and drought losses is found to be nonsignificant in arid and semiarid climate regions in China (*SI Appendix*, Fig. S5 and Table S5).

Besides for the SPEI and PDSI, which are widely used for agro-climatological analysis (18, 30), precipitation-based meteorological index SPI is often used to monitor moisture supply conditions (31). Comparison of time series of SPEI, PDSI, and SPI in China with that of recorded drought losses for 1984–2015 proves that variation of SPEI related closely to the changes of drought losses. A weak correlation between the SPI and drought losses means that not only precipitation but also evapotranspiration and soil moisture play major roles in regional drought development. However, biases in estimation of potential evapotranspiration (PET) under anthropogenic climate change could cause overestimation of drying trends (32, 33). Comparison with the evapotranspiration directly from the climate models at nonwater-stressed condition shows that Penman-Monteith–based analysis is a fair PET estimation method for studying droughts over all of China (*SI Appendix*, Tables S2 and S3).

Under the 1.5 °C global warming scenario, increasing trends of evapotranspiration and precipitation are projected in entire China, but a consistent drying trend is estimated both by SPEI and PDSI mainly in southern China and parts of Northwest China. A few regions in Northeast, North, and Southwest China show trends toward wetter conditions, caused by a stronger impact of increases in precipitation than in evapotranspiration. For an additional 0.5 °C global temperature increase, further intensification of droughts is projected in parts of East, Central, South, Northwest, and Southwest China, with a more pronounced rise in evapotranspiration, leading to more severe dryness conditions (Fig. 1). Considering that the sensitivities of these indices to climate change are different, drought conditions for the 1.5 °C and the 2.0 °C warming levels, deduced by SPI, are also projected to clarify the differences. According to the SPI, averaged coverage and frequency of drought events will decrease due to the increased precipitation in the warming world, but drought intensity is projected to increase for the 1.5 °C and 2.0 °C levels relative to the reference period (*SI Appendix*, Fig. S11).

It becomes clear that absolute drought losses in China will increase under every projected socioeconomic pathway. Along with rapid growth of the socioeconomic conditions, drought losses by the SPI will more than double the observational records in the warming world, but being obviously lower than by other two indices. By the SPEI and PDSI, drought losses will more than triple the records, with more losses for the 2.0 °C target than for the 1.5 °C (*SI Appendix*, Fig. S13 and Tables S6 and S7). The huge increase of losses from droughts by the SPEI and PDSI is due largely to rapid development of future economy, but still attributable to the projected regional dryness trend. Drought losses in the warming climate, for the 1.5 °C and 2.0 °C warming levels, under the assumption of fixed GDP at the year 2010 level, are projected to be, respectively, 48–52% and 58–70% higher than for the recent interval of 2006–2015 (*SI Appendix*, Table S8).

In relation to loss share on the national GDP, a significant decreasing trend was recorded in the recent decades from 0.23% in 1986–2005 to 0.16% in 2006–2015 due to the rapid increase of national GDP. However, the trend was projected to reverse in the future, with this share gradually increasing under the warming climate and possibly approaching the level of the reference period in the 2.0 °C scenario, taking improved adaptation capacity into account. Keeping the increase in global average temperature less than or equal to the 1.5 °C above the preindustrial level can reduce the drought losses almost twofold in China, by several tens of billions of USD (*SI Appendix*, Table S6). Case of drought risks in China presents a clear argument to focus efforts on mitigation, so that the 1.5 °C warming limit is not exceeded.

Data and Methods

Climatic and Socioeconomic Data. Climate projections are based on available ensemble runs by GCMs from CMIP5 (*SI Appendix*, Table S1). Altogether 22 simulations from 13 models, namely GFDL-ESM2M, HadGEM2-ES, IPSL-CM5A-LR, NorESM1-M, CNRM-CM5, MIROC-ESM-CHEM, CanESM2, GFDL-CM3, GFDL-ESM2G, IPSL-CM5A-MR, MIROC-ESM, MIROC5, and MRI-CGCM3, are found to meet the research requirement for calculation of potential evapotranspiration for historical period and future period under RCP2.6 and RCP4.5 scenarios. The GCM outputs were bias-corrected, based on observational data by Equidistant Cumulative Distribution Functions (EDCDF) method and downscaled statistically to a regular geographical grid with a 0.5° resolution by the spatial disaggregation (SD) method. The bias correction and statistical downscaling lead to an improvement of GCMs in reproducing the observed spatial pattern and long-term average of climatic variables (*SI Appendix*, Figs. S2–S4), and thus, intensity of drought events can be also well captured by GCMs (*SI Appendix*, Fig. S6).

Observational gridded dataset of climate variables (daily precipitation, temperature, relative humidity, wind speed, shortwave radiation estimated by the sunshine duration) with 0.5° resolution used as a reference in the downscaling method is constructed in the National Climate Center of China Meteorological Administration based on nearly 2,400 ground-based stations in China by means of the "anomaly approach" method (34).

County-level socioeconomic data for 1984–2015 in China stem from the China Statistical Yearbook (35). The data are interpolated into a geographical grid corresponding to the 0.5° resolution of the GCM's outputs using the area-weighted interpolation method. Provincial scale GDP in China under SSPs for 2010–2060 is projected by Cobb–Douglas production model with regionalized parameters, including labor force, total factor productivity, and capital stock. The latest universal two-child policy in China is fully considered for labor force projection, and initial information on fertility, deaths, migration, total factor productivity, and capital stock, are from the latest demographical and economic census. The parameterization scheme for SSP1–5 is followed in refs. 12 and 36. To maintain the homogeneity of the data series, GDPs recorded

in 1986–2015 and projected in 2010–2060 are standardized to 2015 prices (*SI Appendix*, Fig. S7). Gridded GDP for the period 2010–2060 is derived by scaling the provincial GDP projections to 0.5° resolution, based on the weights of individual grid cells to the entire provincial GDP, which are deduced from the observational period (37).

Droughts and their direct economic losses are recorded once an event with coverage ≥50,000 km^2 and duration ≥20 d happened in any province from 1984 to 2015 (24). The datasets are checked and ratified by Ministry of Civil Affairs and National Committee for Disaster Reduction in China with data from several sectors, including China Meteorological Administration, Ministry of Agriculture, Ministry of Water Resources, and National Bureau of Statistics.

Identification of Drought Events. Drought events are identified according to the SPEI, PDSI, SPI, and the cluster analysis method. The SPEI approach proposed in ref. 18 is the standardization of the difference between precipitation and potential evapotranspiration, while the SPI developed in ref. 31 is used to quantify the precipitation deficits or surpluses only. The self-calibrated PDSI (20, 21) is based on the supply and demand model of soil moisture. In this study, potential evapotranspiration in both the SPEI and PDSI is deduced with the Penman–Monteith equation (38), as recommended by the Food and Agriculture Organization (FAO). Available water holding capacity required for the PDSI actual evapotranspiration is provided by the Potsdam Institute for Climate Impact Research using the FAO digitized soil map (39). For detailed information on the way of potential and actual evapotranspiration calculation, see *SI Appendix*, SI2. Parameters included in calculation process of the drought indices are estimated in the reference period and then used in the future to make sure that the dryness or wetness conditions in the warming levels are based on the status in the reference period.

Drought indices are calculated for a monthly time scale at each grid. Dryness is diagnosed once SPEI ≤ −1, PDSI ≤ −2 or SPI ≤ −1, and the lower the value of SPEI, PDSI, or SPI, the more severe the dryness condition (*SI Appendix*, Table S4). A cluster analysis method is used to identify the drought events (8, 22, 40, 41) by determining the drought center (grid with maximum intensity) first and then clustering all neighboring grid cells that fit the drought criteria of SPEI ≤ −1, PDSI ≤ −2, or SPI ≤ −1. Summed area of clustered grids is the areal coverage of a drought event, and averaged value of drought indices over the summed area is the intensity of a drought event (*SI Appendix*, SI3). As the drought events and losses recorded in the meteorological disaster yearbook of China only refer to events covering an area larger than 50,000 km^2, drought events of a smaller spatial scale are not considered in this study.

Intensity-Loss Rate Function. To estimate the losses caused by drought events of different intensities, the intensity-loss rate curves are set up for each province in China based on the direct economic losses of droughts during the period 1984–2015, which are recorded in the yearbook of meteorological disasters in China (24). For each province, the drought intensity is averaged for all drought events per year. The loss rate is the ratio between annual drought losses and GDP in drought areal coverage in a province. For reflecting the improved adaptation capacity to cope with meteorological disaster in the future, the slope of the intensity-loss rate curve is designed to change together with socioeconomic condition (*SI Appendix*, SI6). The intensity-loss rate, combined with future drought exposure and projected drought intensity, is used for the estimation of future drought losses.

ACKNOWLEDGMENTS. We thank the World Climate Research Programme's working group on coupled modeling for producing and making available their model output, and the constructive advice of Dr. P. C. D. Milly is gratefully acknowledged. This study is jointly supported by National Key R&D Program of China Grant 2017YFA0603701, National 1000 Talent Program Grant Y474171, and National Natural Science foundation of China Grants 41671211 and 41661144027.

1. Handmer J, et al. (2012) Changes in impacts of climate extremes: Human systems and ecosystems. *Managing the Risks of Extreme Events and Disasters to Advance Climate Change Adaptation. A Special Report of Working Groups I and II of the Intergovernmental Panel on Climate Change (IPCC)*, eds Field CB, et al. (Cambridge Univ Press, Cambridge, UK), pp 231–290.
2. EM-DAT (2017) EM-DAT: The OFDA/CRED international disaster database (Univ Catholique de Louvain, Brussels). Available at https://www.emdat.be. Accessed September 15, 2018.
3. Dai A (2013) Increasing drought under global warming in observations and models. *Nat Clim Change* 3:52–58.
4. Trenberth KE, et al. (2014) Global warming and changes in drought. *Nat Clim Change* 4:17–22.
5. Dai A, Zhao T (2016) Uncertainties in historical changes and future projections of drought. Part I: Estimates of historical drought changes. *Clim Change* 144:519–533.
6. Fischer T, Gemmer M, Liu L, Su BD (2011) Temperature and precipitation trends and dryness/wetness pattern in the Zhujiang River Basin, South China, 1961-2007. *Quat Int* 244:138–148.
7. Chen HP, Sun JQ (2015) Changes in drought characteristics over China using the standardized precipitation evapotranspiration index. *J Clim* 28:5430–5447.
8. Zhai JQ, et al. (2017) Intensity- area-duration analysis of droughts in China 1960-2013. *Clim Dyn* 48:151–168.
9. Sheffield J, Wood EF (2008) Projected changes in drought occurrence under future global warming from multi-model, multi-scenario, IPCC AR4 simulations. *Clim Dyn* 31:79–105.
10. UNFCCC (United Nations Framework Convention on Climate Change) (2015) Report of the ad hoc working group on the Durban platform for enhanced action on the eighth part of its second session, held in Geneva from 8 to 13 February 2015 (United Nations, Geneva), Technical Report FCCC/ADP/2015/2.
11. IPCC (Intergovernmental Panel on Climate Change) (2013) *Summary for Policymakers. Climate Change 2013: The Physical Science Basis. Contribution of Working Group I to the Fifth Assessment Report of the Intergovernmental Panel on Climate Change*, eds Stocker TF, et al. (Cambridge Univ Press, Cambridge, UK).
12. Leimbach M, Kriegler E, Roming N, Schwanitz J (2017) Future growth patterns of world regions–A GDP scenario approach. *Glob Environ Change* 42:215–225.
13. Warszawski L, et al. (2014) The inter-sectoral impact model intercomparison project (ISI–MIP): Project framework. *Proc Natl Acad Sci USA* 111:3228–3232.
14. Burke EJ, Brown SJ (2008) Evaluating uncertainties in the projection of future drought. *J Hydrometeorol* 9:292–299.
15. Orlowsky B, Seneviratne SI (2013) Elusive drought: Uncertainty in observed trends and short- and long-term CMIP5 projections. *Hydrol Earth Syst Sci* 17:1765–1781.
16. Touma D, Ashfaq M, Nayak MA, Kao SC, Diffenbaugh NS (2015) A multi-model and multi-index evaluation of drought characteristics in the 21st century. *J Hydrol* 526:196–207.
17. Sun QH, Moa CY, Duan QY (2015) Projected changes in temperature and precipitation in ten river basins over China in 21st century. *Int J Climatol* 35:1125–1141.
18. Vicente-Serrano SM, Beguería S, Lopez-Moreno JI (2010) A multiscalar drought index sensitive to global warming: The standardized precipitation evapotranspiration index. *J Clim* 23:1696–1718.
19. Beguería S, Vicente-Serrano SM, Reig F, Latorre B (2014) Standardized precipitation evapotranspiration index (SPEI) revisited: Parameter fitting, evapotranspiration models, tools, datasets and drought monitoring. *Int J Climatol* 34:3001–3023.
20. Palmer WC (1965) Meteorological drought, U.S. Weather Bureau Research Paper No. 45 (US Government Printing Office, Washington, DC).
21. Wells N, Goddard S (2004) A self-calibrating palmer drought severity index. *J Clim* 17: 2335–2351.
22. Sheffield J, Andreadis KM, Wood EF, Lettenmaier DP (2009) Global and continental drought in the second half of the twentieth century: Severity-area-duration analysis and temporal variability of large scale events. *J Clim* 22:1962–1981.
23. Xu K, et al. (2015) Spatio-temporal variation of drought in China during 1961-2012: A climatic perspective. *J Hydrol* 526:253–264.
24. China Meteorological Administration (2016) *Yearbook of Meteorological Disasters in China* (China Meteorolog Press, Beijing).
25. Hirabayashi Y, et al. (2013) Global flood risk under climate change. *Nat Clim Change* 3:816–821.
26. O'Neill BC, et al. (2017) The roads ahead: Narratives for shared socioeconomic pathways describing world futures in the 21st century. *Glob Environ Change* 42:169–180.
27. van Vuuren DP, et al. (2014) A new scenario framework for climate change research: Scenario matrix architecture. *Clim Change* 122:373–386.
28. Sheffield J, Wood EF, Roderick ML (2012) Little change in global drought over the past 60 years. *Nature* 491:435–438.
29. Wang AH, Lettenmaier DP, Sheffield J (2011) Soil moisture drought in China, 1950-2006. *J Clim* 24:3257–3271.
30. Alley WM (1984) The Palmer drought severity index: Limitations and assumptions. *J Clim Appl Meteorol* 23:1100–1109.
31. McKee TB, Doesken NJ, Kleist J (1993) The relationship of drought frequency and duration to time scales. *Proceedings of the Eighth Conference on Applied Climatology* (Am Meteorolog Soc, Boston), pp 179–184.
32. Milly PCD, Dunne A (2017) A hydrologic drying bias in water-resource impact analyses of anthropogenic climate change. *J Am Water Resour Assoc* 53:822–838.
33. Milly PCD, Dunne A (2016) Potential evapotranspiration and continental drying. *Nat Clim Change* 6:946–950.
34. Wu J, Gao XJ (2013) A gridded daily observation dataset over China region and comparison with the other datasets. *Chin J Geophys* 56:1102–1111.
35. National Bureau of Statistics of China (2016) *China Statistical Yearbook 2015* (China Stat Press, Beijing).
36. Kc S, Lutz W (2017) The human core of the shared socioeconomic pathways: Population scenarios by age, sex and level of education for all countries to 2100. *Glob Environ Change* 42:181–192.
37. Jiang T, et al. (2018) National and provincial economic change projected to 2100 under the Shared Socioeconomic Pathways in China. *Adv Clim Chang Res* 14:50–58.
38. Allen RG, Pereira LS, Raes D, Smith M (1998) *Crop Evapotranspiration–Guidelines for Computing Crop Water Requirements–FAO Irrigation and Drainage Paper 56* (Food and Agric Org, Rome).
39. FAO (1991) *The Digitized Soil Map of the World (Release 1.0)* (Food and Agric Org, Rome).
40. Andreadis KM, Clark EA, Wood AW, Hamlet AF, Lettenmaier DP (2005) Twentieth-century drought in the conterminous United States. *J Hydrometeorol* 6:85–101.
41. Huang JL, et al. (2017) Analysis of future drought characteristics in China using the regional climate model CCLM. *Clim Dyn* 50:507–525.

Supplementary Information

The supplementary material contains additional 13 figures and 8 tables.

SI 1: Model outputs

Temperature (mean, maximum, minimum), as well as relative humidity, wind speed and shortwave radiation, is required for the calculation of potential evapotranspiration. All necessary variables for drought analyses both in the historical period and the warming level under RCP2.6 and RCP4.5 scenarios are available for 22 ensemble runs from 13 GCMs in CMIP5 (Table S1). To obtain a credible dataset at regular geographical resolution of 0.5° (Fig.S1), GCM outputs with different resolutions are bias corrected and statistically downscaled.

Table S1 models and modeling groups

Model name	Ensemble runs	Modeling group	Grid resolution (Longitude×Latitude)
CNRM-CM5	r1i1p1	Centre National de Recherches Meteorologiques/Centre European de Recherche et Formation Avancees en Calcul Scientifique	1.40625°×1.4008°
CanESM2	r1i1p1, r2i1p1, r3i1p1, r4i1p1, r5i1p1	Canadian Centre for Climate Modelling and Analysis	2.8125°×2.7906°
GFDL-CM3	r1i1p1	Geophysical Fluid Dynamics Laboratory	2.5°×2.0°
GFDL-ESM2G	r1i1p1		2.0°×2.0225°
GFDL-ESM2M	r1i1p1		2.5°×2.0225°
HadGEM2-ES	r1i1p1	Met Office Hadley Centre	1.875°×1.25°
IPSL-CM5A-LR	r1i1p1, r2i1p1, r3i1p1, r 4i1p1	Institute Pierre-Simon Laplace	3.75°×1.8947°
IPSL-CM5A-MR	r1i1p1		2.5°×1.2676°
MIROC-ESM	r1i1p1	Japan Agency for Marine-Earth Science and Technology, Atmosphere and Ocean Research Institute (The University of Tokyo), and National Institute for Environmental Studies	2.8125°×2.7906°
MIROC-ESM-CHEM	r1i1p1		2.8125°×2.7906°
MIROC5	r1i1p1, r2i1p1, r3i1p1		1.40625°×1.4008°
MRI-CGCM3	r1i1p1	Meteorological Research Institute	1.125°×1.12148°

www.pnas.org/cgi/doi/10.1073/pnas.1802129115

NorESM1-M	r1i1p1	Norwegian Climate Centre, Norway	2.5°×1.8947°

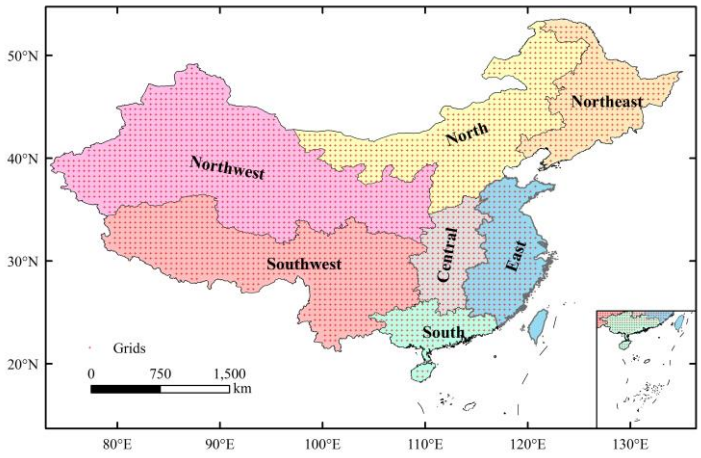

Fig.S1 Location of grids with 0.5° geographical resolution in the seven sub-regions in China

Based on the bias between modeled and observed climatic variables at each percentile (Δ in Fig. S2), a method of Equidistant Cumulative Distribution Functions (EDCDF) is used to adjust the Cumulative Distribution Function (CDF) of simulation datasets (1). Normal distribution and beta distribution is fitted to temperature and relative humidity field, respectively, and a mixed gamma distribution is fitted to precipitation and other climatic variables including wind speed and shortwave radiation. EDCDF assumes that the difference between observed and modeled values during the training period maintains in the correction period for a given percentile. The EDCDF method (Fig. S2) can be written as:

$$\Delta = F_{oc}^{-1}(F_{ms}(x)) - F_{mc}^{-1}(F_{ms}(x))$$

$$x_{correct} = x + \Delta$$

Here, x is climatic variable; F is the cumulative distribution function (CDF) and F^{-1} is the inverse CDF; *oc* denotes observations in the training period; *mc* denotes model outputs in the training period; *ms* denotes model outputs in a correction period.

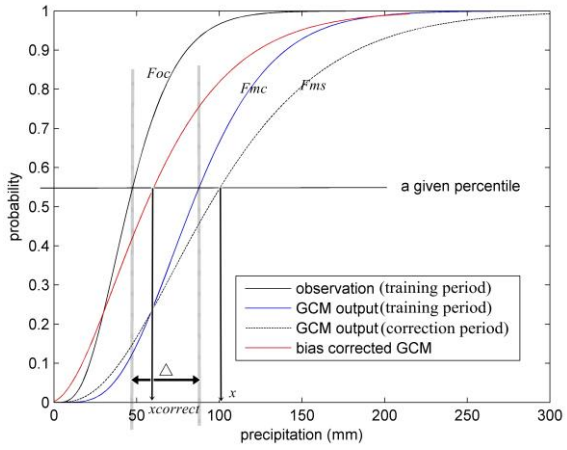

Fig. S2 Demonstration of EDCDF bias correction method (takes precipitation output from GFDL-ESM2G model in May as an example. grid location: 39.4382°N, 133.75°E)

Spatial Disaggregation (SD) statistical downscaling method (2) is adopted to bias corrected series to produce high-resolution outputs. SD is conducted based on the assumption that the topographic and the climatic features determined fine-scale distribution of large-scale climate will remain unchanged in the future periods. At the first step, 0.5°gridded observational climate variables over China are interpolated to GCM coarse resolution using bilinear interpolation method based on their multi-year averaged mean. Anomaly fields between the observational climate variables and bias corrected model outputs for temperature is defined as the difference between simulated and observed data, and for precipitation, wind speed, relative humidity and shortwave radiation, is the ratio of model output to observational data. At the second step, the coarse resolution anomaly fields of climate variables are interpolated to 0.5° resolution using bilinear interpolation method, and the interpolated anomaly fields are applied to 0.5°gridded observational climate variables to get the downscaled GCM simulations.

After bias correction and statistically downscaled by applying the EDCDF and SD methods, GCMs' capabilities for describing regional climate pattern over China is improved obviously. Takes simulated wind speed from a GCM (GFDL-ESM2G) as an example, it is clear that spatial pattern of mean annual wind speed in 1986-2005 is not well captured by the GCM. Besides for a systematic underestimation, less than 0.3 of spatial correlation coefficient between simulated and observed wind speed is found (Figs.S3a-b). Conduction of bias correction for each grid in China substantially increase the spatial correlation coefficient to above 0.9 (Fig.S3c), and more detailed spatial information is obtained by the statistical downscaling (Fig.S3d). The multi-year averaged wind speed output in 1986-2005 from the GCM is increased from 1.37 m/s to about 2.29 m/s after bias correction and downscaling, reaching closer to that of 2.32 m/s from observation (Fig.S4).

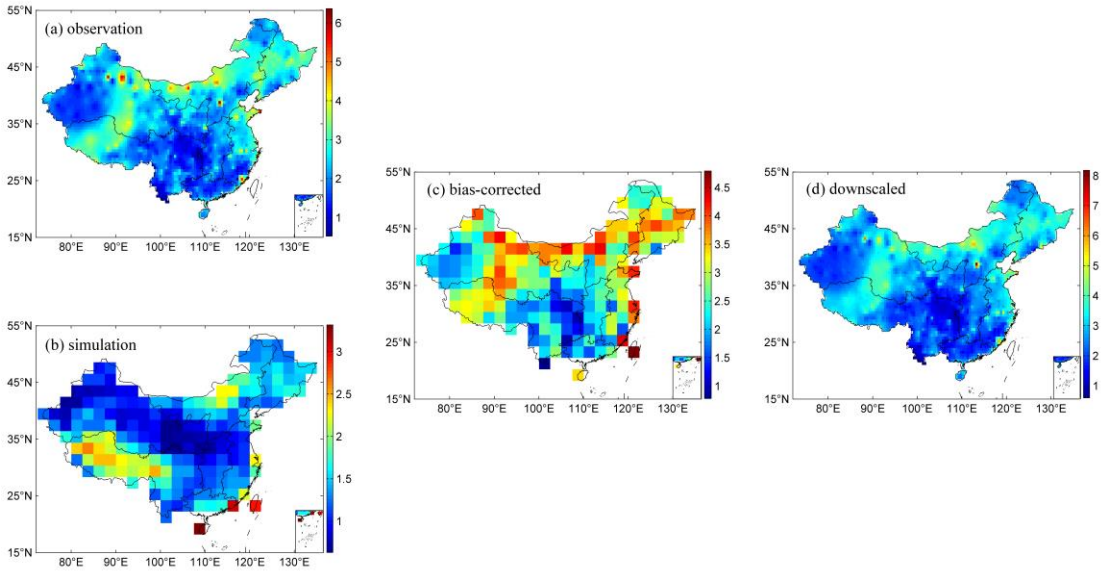

Fig. S3 Comparison of observed wind speed (a), original GCM output (b), bias-corrected GCM output (c), bias-corrected and downscaled GCM output (d) in the period of 1986-2005 (unit: m/s) (takes annual mean wind speed output from GFDL-ESM2G model as an example)

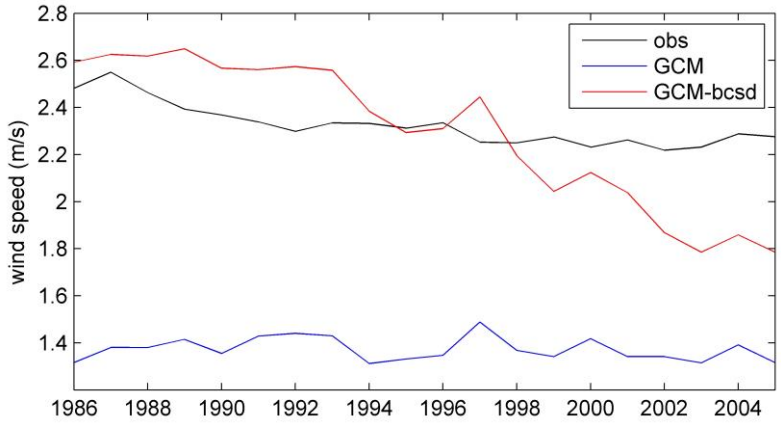

Fig. S4 Comparison of observed annual mean wind speed, original GCM output with bias corrected and statistically downscaled GCM result in 1986-2005 in China

SI 2: Drought indices

The standardized precipitation index (SPI) is used to quantify the precipitation deficits or surpluses by fitting long-term precipitation record to a gamma distribution (3), and the standardized precipitation-evapotranspiration index (SPEI) is calculated by normalizing the differences between precipitation and Potential evapotranspiration (PET) into a log-logistic probability distribution (4).

$$SPI = norminv(CP\_P)$$
$$CP\_P = (1 - q0) * Gamcdf(P0) + q0$$
$$SPEI = norminv(CP\_D)$$
$$D_i = P_i - PET_i$$

Here, *norminv* is the standardization function. *CP_P* is cumulative probability of *precipitation*, and *CP_D* is cumulative probability of *D*. *Gamcdf* is the gamma cumulative distribution function. *q*0 is the probability of zero precipitation. *P*0 is the precipitation without zero values. *CP_D* is obtained based on the log-logistic probability distribution.

The Palmer drought severity index (PDSI) is based on the supply and demand model of soil moisture (5, 6). Soil model is a two-stage "bucket" model, and precipitation, PET, latitude of the location of interest, and available water holding capacity (AWC) are needed in the calculation. AWC is known as the field capacity and calculated in the Potsdam Institute for Climate Impact Research according to the soil type datasets from FAO.

$$PDSI_i = p * PDSI_{i-1} + q * Z_i$$
$$Z = (P - Pc) * K$$
$$Pc = \alpha_i * PE + \beta_i * PRE + \gamma_i * PRO - \delta_i * PL$$
$$\alpha_i = \frac{\overline{ET_\iota}}{\overline{PET_\iota}},\ \beta_i = \frac{\overline{R_\iota}}{\overline{PR_\iota}},\ \gamma_i = \frac{\overline{RO_\iota}}{\overline{PRO_\iota}},\ \delta_i = \frac{\overline{L_\iota}}{\overline{PL_\iota}}$$

Here, *Z* is moisture anomaly index, *i* is given month, *P* is actual precipitation and *Pc* is climatically appropriate for existing conditions (CAFEC) precipitation. *K* represents climatic characteristic. *p*

and q are the duration factors, and can be obtained based on the historical climate. *Pc* are decided by the water balance coefficients α, β, γ, δ and PET, potential recharge to soils(*PR*), potential runoff(*PRO*), potential loss (*PL*). *ET*, *RE*, *RO* and *L* denote evapotranspiration, recharge, runoff and loss respectively.

SI 3: Estimation of potential and actual evapotranspiration

Previous studies show that increase of PET with anthropogenic climate change seems to be overestimated by all existing PET functions except for the energy-only method (8, 9). Theoretically, PET is equal to ET in the non-water-stressed conditions. We deduced PET in the non-water-stressed conditions in China following various methods suggested by Milly and Dunne (Table S2), and compare them with evapotranspiration output directly from climate models. The non-water-stressed locations and months are identified once the slope of parabola (when ET and precipitation is fitted by a parabola) is less than 0.05 and ratio of ET and precipitation is less than 2.

As shown in Table S3, PET by Thornthwaite, Hamon and Penman-Monteith methods approach most closely with the values of non-water-stressed evapotranspiration (Ew) in climate models. Meanwhile, changes of Ew in the warming world can be well captured by Penman-Monteith, but Thornthwaite and Hamon equations overestimate the relative changes. We also found that Priestley-Taylor method can reproduces the relative changes in Ew in climate models. Priestley-Taylor equation is similar to the energy component in Penman equation， and using an empirically determined coefficient to denote the proportionality between PET and available energy. This empirically determined coefficient $\alpha \approx 1.3$ is supported by plentiful experiments at non-water-limiting regions. But, the Priestley-Taylor method with the constant empirical coefficient is not applicable in arid and semi-arid areas, where PET is possibly affected by the advection and neglecting of advection would lead to a substantial underestimate (9-12). Thus, PET in this study is deduced by the Penman-Monteith equation recommended by FAO (13).

Table S2 Equations of Potential evapotranspiration

PET method	Equation	Other unknown parameters
Oudin (11)	$PET = 0.4\,R_s\,\frac{max\,(T+5,0)}{100}$	-
Hargreaves-Samani (12)	$PET = \frac{0.00094}{1000000} \times\ 0.4\,(32+1.8\,T)\sqrt{1.8(T_{max}-T_{min})}$	-
Thornthwaite (13)	$PET = 16\,\frac{N}{12}\,\frac{NDW}{30}\left(\frac{10\,max(T_m,0)}{I}\right)^{\alpha}\ (if\ T_m < 26.5)$ $PET = \left(-415.85+32.24\,T_m - 0.43\,{T_m}^2\right)\frac{N}{12}\,\frac{NDW}{30}\ (if\ T_m \geq 26.5)$	*N* is number of daylight hours, *NDW* is number of days in the month, T_m is average

	$I = \sum_{i=1}^{12} max\ (T_m, 0)^{1.514}$ $\alpha = 0.000000675\ I^3 - 0.0000771\ I^2 + 0.01792\ I + 0.49239$	temperature for each month.
Hamon (14)	$PET = \frac{6.5}{25.4}\ \frac{N}{12}\ \frac{1000\ e_s}{461.5\ (T + 273.2)}$	N is the daylight hours
Penman-Monteith (7)	$PET = \frac{0.408\Delta(R_n - G) + r\frac{900}{T + 273.16}U_2(e_s - e_a)}{\Delta + r(1 + 0.34U_2)}$	-
Penman (15)	$PET = 0.4\ \frac{\Delta}{\Delta + \gamma}(R_n - G) + \frac{0.4}{1000}\frac{\gamma}{\Delta + \gamma}\ 6.43\ (1 + 0.536\ U_2)\ (e_s - e_a)$	-
Priestley-Taylor (16)	$PET = 1.26\ \times 0.4\ \frac{\Delta}{\Delta + \gamma}(R_n - G)$	-
Energy Only (8, 9)	$PET = 0.8\ \times 0.4\ (R_n - G)$	-

Table S3 Comparison of PET estimated by different equations and ET direct outputs from climate models for non-water stressed grids-months for the 1.5℃ and 2.0℃ warming period and the reference period (1986-2005). Values in Table are the multi-model ensemble mean

	Ref. (mm/month)	1.5 ℃ (mm/month)	2.0℃ (mm/month)	Relative changes between 1.5 ℃and reference (mm/month)	Relative changes between 2.0℃and reference (mm/month)	Relative changes between 2.0℃ and 1.5℃ (mm/month)
Oudin	28.4	31.0	33.0	2.6	4.6	2.0
Hargreaves-Samani	34.9	36.9	38.9	2.0	4.0	2.0
Thornthwaite	55.0	60.7	63.5	5.7	8.5	2.8
Hamon	56.4	62.0	64.5	5.6	8.1	2.5
Penman-Monteith	67.9	71.0	74.0	3.1	6.1	3.0
Penman	79.6	82.7	86.0	3.1	6.4	3.3
Priestley-Taylor	84.4	86.9	90.4	2.5	6.0	3.5
Energy only	89.6	88.7	90.8	-0.9	1.2	2.1
Climate model	59.4	61.5	65.3	2.1	5.9	3.8

Temperature (mean, maximum, minimum), as well as air pressure, relative humidity, wind speed and sunshine duration/ shortwave radiation are required to deduce Penman-Monteith PET. Reference crop is assumed with crop height of 0.12 m, a fixed surface resistance of 70 s/m and an albedo of 0.23.

$$PET = \frac{0.408\Delta(R_n - G) + r\frac{900}{T+273.16}U_2(e_s - e_a)}{\Delta + r(1+0.34U_2)}$$

Here, R_n is the net radiation at the crop surface (unit: MJ/m^2/day) ; G is soil heat flux density (MJ/m^2/day), which is negligible at daily time scale; T denotes mean air temperature at 2 m height (^{o}C); U_2 is the wind speed at 2m height (m/s); e_s is saturation vapour pressure (kPa), estimated by daily maximum temperature and minimum temperature; e_a is actual vapour pressure (kPa), calculated by maximum temperature, minimum temperature and relative humidity datasets; Δ is the slope vapour pressure curve (kPa/ ^{o}C), which can be estimated by the daily mean tempearture; r is the psychrometric constant (kPa/ ^{o}C), estimated by the atmospheric pressure.

R_n, net radiation, is the difference between the incoming net shortwave radiation (R_{ns}) and the outgoing net longwave radiation (R_{nl}):

$$R_n = R_{ns} - R_{nl}$$

$$R_{ns} = (1 - a)R_s$$

$$R_{nl} = \sigma\left[\frac{(T_{max}+273.16)^4 + (T_{min}+273.16)^4}{2}\right]\left(0.34 - 0.14\sqrt{e_a}\right)\left(1.35\frac{R_s}{R_{so}} - 0.35\right)$$

Here, a is the albedo or canopy reflection coefficient (0.23); R_s is the incoming solar radiation; σ is the Stefan-Boltzmann constant (4.903×10^{-9} MJ/K^4/m^2/day); T_{max} is the daily maximum temperature (unit: ^{o}C); T_{min} is the daily minimum temperature (unit: ^{o}C); e_a is actual vapour pressure; R_{so} is clear sky solar radiation.

$$R_s = (a_s + b_s\frac{n}{N})R_a$$

$$R_{so} = (0.72 + 2 \times 10^{-5}z)R_a$$

$$R_a = \frac{24(60)}{\pi}G_{sc}d_r[(\omega_s\, sin\varphi\, sin\delta) + (cos\varphi\, cos\delta\, sin\omega_s)]$$

Here, R_a is the extraterrestrial radiation; G_{sc} is solar constant (0.0820 MJ/m^2/min); d_r is the inverse relative distance Earth-Sun and δ is the solar declination; ω_s is sunset hour angle, estimated by latitude φ (radians) and solar declination δ ; z is elevation above sea level (unit: m); a_s and b_s is recommend as 0.25 and 0.50, respectively, when the empirical parameters are missing; n is sunshine duration; N is the maximum possible sunshine duration, calculated by the sunset hour angle ω_s.

Actual evapotranspiration (*ET*) is estimated in a two-layer "bucket" model of the soil. Soil moisture storage is handled by dividing the soil into two layers and assuming that 1 inch of water can be stored in the surface layer. If there is sufficient precipitation to satisfy the PET requirement for a month, the *ET* would be equal to the *PET*. When the precipitation is less than the *PET*, the ET is the difference between precipitation and soil moisture loss from both the surface and underlying soil layers.

$$ET = PET \qquad if\ P > PET$$

158 $$\begin{cases} ET = P + Ls + Lu \\ Ls = Ss - (PET - P) \\ Lu = 0 \end{cases} \quad if\ P < PET, Ss > PET - P$$

159 $$\begin{cases} ET = P + Ls + Lu \\ Ls = Ss \\ Lu = Su - (PET - P - Ss) \end{cases} \quad if\ P < PET, Ss < PET - P$$

160 Here, *Ls* is soil moisture loss from the surface; *Lu* is soil moisture loss from the underlying soil
161 layer; *Ss* is soil moisture in surface layer; *Su* is soil moisture in the underlying soil layer. The
162 calculation is initialized during a month when the soil moisture storage assumed to be full. The
163 initial soil moisture storage is 1 in the surface soil layer, and 'field capacity'-1 in the underlying soil
164 layer.

165 **SI 4: Identification and validation of drought events by different indices**

166 Drought conditions are identified for each grid according to SPEI, PDSI, SPI values, and drought
167 event can be clustered by considering the feature of drought intensity, area, and duration. In this
168 study, droughts are identified by monthly scale by criteria of SPEI≤-1, PDSI≤-2, SPI≤-1 (Table S4).
169 Starts from the drought center, which is a grid with the lowest SPEI, PDSI or SPI value, Intensity-
170 Area-Duration analysis (17, 18) is conducted using the cluster algorithm, by attaching the adjacent
171 grids which meet the threshold of SPEI≤-1, PDSI≤-2, SPI≤-1 to the drought center. The processes
172 will be iterated until no any adjacent grid meets the drought criteria. Total coverage and averaged
173 drought indices over the clustered grids is the area and intensity of a drought event, respectively.
174 For each cluster, the events with area less than 50,000 km^2 are not included in the statistics (19).
175
176 Table S4 Classification of dryness degree in accordance with the SPEI, PDSI and SPI definitions

Categories	SPEI (and SPI)	PDSI
Near Normal	-0.99 ~ 0	-1.99 ~ 0
Moderately dry	-1.49 ~ -1.0	-2.99 ~ -2.0
Severely dry	-1.99 ~ -1.5	-3.99 ~ -3.0
Extreme dry	≤ -2.0	≤ -4.0

177
178 Time-series of dry and wet conditions by different drought indices in historical period of 1984-2015
179 in China are calculated using observational data and compared with recorded drought losses
180 standardized by CPI in Fig. S5 and Table S3. View China as a whole, it is found that all three applied
181 indices are highly correlated with each other with correlation coefficient higher than 0.75. No
182 significant dryness change is detected by the PDSI during 1984-2015, which is in line with drought
183 trend represented by the soil moisture in China (20) and regional character of droughts in a global
184 study using same drought index (21), but a significant dryness change is found by the SPEI. Among
185 three indices, SPEI related closely with the drought losses with a correlation coefficient of -0.61.
186 On the contrary, weak correlation with drought losses is found by SPI. In addition, slope of SPEI,
187 SPI and PDSI are -0.089/10a, -0.004/10a and -0.049/10a for 1984-2015, indicating a less drying
188 trend by SPI. The ignoring of water balance elements of evapotranspiration or soil moisture might
189 lead to an underestimation of the dryness conditions, especially in the future as the surface
190 temperature projected to increase furthermore (22).

In the humid and semi-humid regions of China, where annual precipitation is above 400mm, both SPEI and PDSI are highly correlated with drought losses, capable of representing the regional drought conditions. However, only SPEI show a significant relationship with losses in the arid and semi-arid regions, where annual precipitation in vast area is less than 200mm (Table S5). In addition, aggravation of droughts is detected by the SPEI in the arid and semi-arid regions, while a weak wetting trend is found by the PDSI (Fig. S5c).

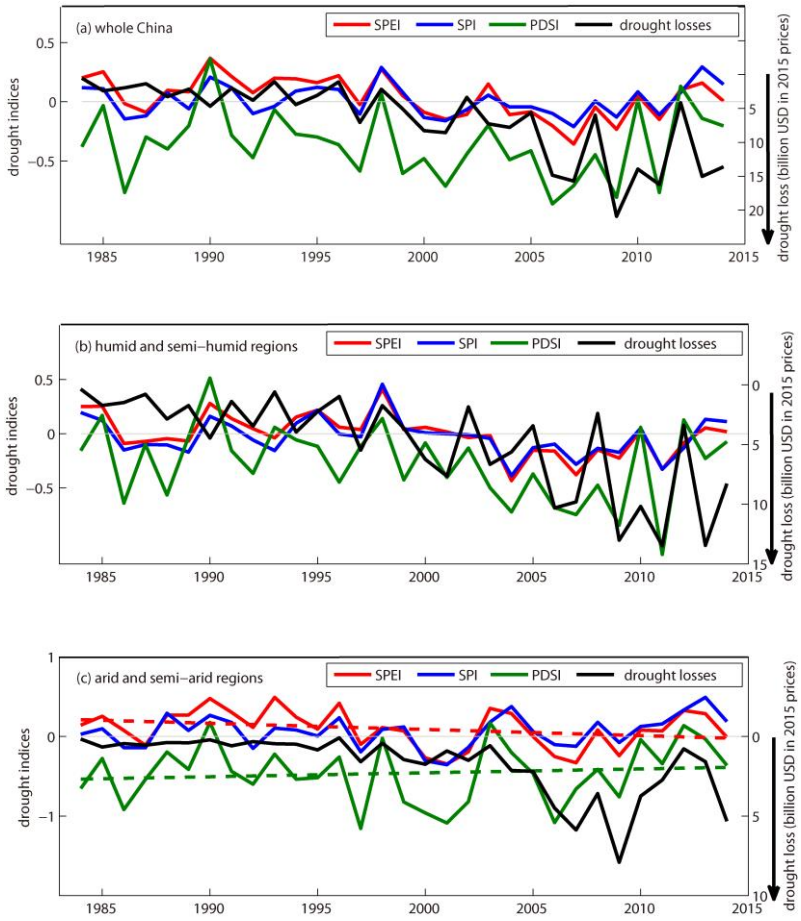

Fig. S5 Comparison of drought indices (SPEI, SPI, PDSI) in China and their relationship with the recorded drought losses corrected by CPI for 1984-2015 (right vertical axis is reversed). Dotted lines in (c) are the slopes of SPEI and PDSI indices.

Table S5 Pearson's correlation coefficients among drought indices (SPEI, SPI, PDSI) and recorded drought losses

		SPEI	SPI	PDSI	Loss
Whole China	SPEI	1	0.80**	0.78**	-0.61**
	SPI		1	0.79**	-0.23
	PDSI			1	-0.32
Humid and semi-humid regions	SPEI	1	0.94**	0.74**	-0.44*
	SPI		1	0.65**	-0.25
	PDSI			1	-0.46**

Arid and semi-arid regions	SPEI	1	0.77**	0.76**	-0.57**
	SPI		1	0.81**	-0.12
	PDSI			1	-0.23

(**: significant at 0.01 level, *: significant at 0.05 level)

SI 5: Comparison of drought intensities deduced by GCM outputs and observed data

In 1986-2005, averaged intensity of drought events over China as deduced by the SPEI and the PDSI from GCM outputs is -1.83 and -3.6, respectively, both are close to that from observational data (-1.81 and -3.53), entails that intensity of drought events in China can be well captured by bias corrected and downscaled GCMs (Fig.S6).

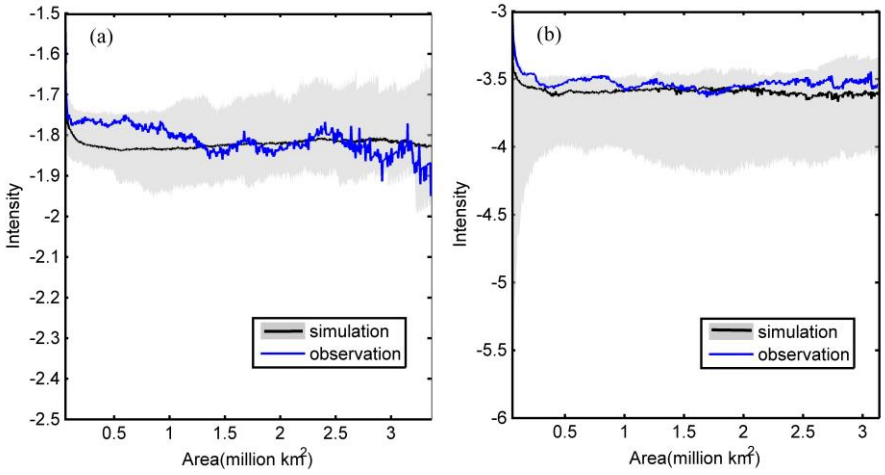

Fig. S6 Averaged drought intensity at different contiguous drought areas in China for 1986-2005 by GCM simulations and observation. Drought characteristics in (a) and (b) are deduced by the SPEI and PDSI, respectively. Shadows and lines in (a, b) are the bands and median, respectively, by twenty-two GCM runs.

SI 6: Projection of economy in China for the 21st century

To date, projections of the SSP's population and GDP are available only at the country level from the Organization for Economic Co-operation and Development (OECD) for the period 2010-2100 in 10-year time steps (23). In current study, GDP in China for SSPs is updated with regionalized parameters by using Cobb-Douglas production model annually, and standardized to 2015 price to maintain the homogeneity of data series. It is projected that GDPs under SSP1-5 stay close to each other until around 2030. Since then, constant increases of GDP are projected under SSP2, SSP3 and SSP5, but visible differences are found between the SSP5 (highest) and SSP3 (lowest) pathways. Under SSP1 and SSP4, GDP will reach at peak in 2080s and 2070s, respectively. Trajectory of GDP under SSP2 lies at the middle (Fig. S7).

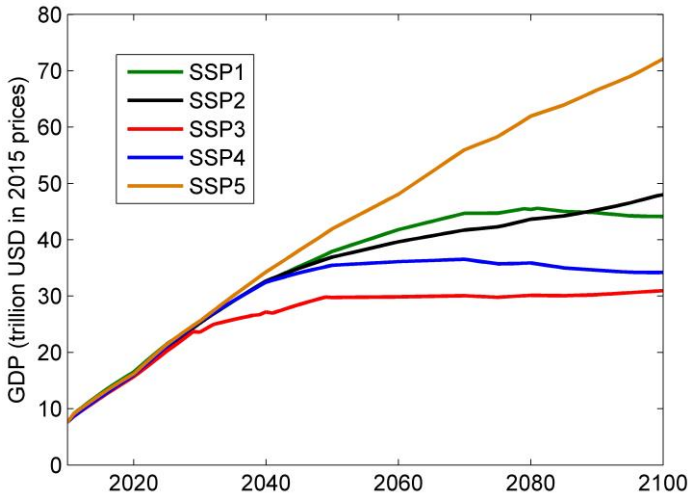

Fig. S7 Projections of GDP in China under SSPs

SI 7: Development of "intensity-loss rate" curve in changing socioeconomic condition

For estimation of the direct economic loss caused by droughts, the "intensity-loss rate" curves are set up for each province in China, based on the drought losses recorded in the yearbook of meteorological disasters in China during the period 1984-2015. In Figs. S8-S9, the horizontal axis is the drought intensity (I), denotes the averaged intensity of total drought events per year indentified by SPEI or PDSI at each province. Vertical axis is the loss rate (r) , denotes the ratio between annual drought losses and provincial GDP exposed to droughts. Relationship between I and r are fitted by the Napierian Logarithm function:

$$r = a * \ln(-I + 1)$$

The slope (a) at the "intensity-loss rate" curve is an indicator of the adaptation capacity. Provinces with lower a usually encounter a lower loss than those with higher a when facing droughts with similar intensities. With the development of socioeconomy, the adaption capacity of human beings to meteorological disasters, such as droughts, will increase. For reflecting the improved adaptation capacity to cope with meteorological disasters in the future, slope (a) of the curves in Figs. S8-S9 within China was linked with provincial GDP per unit area in 1984-2015 to show how the regional development affects the adaption capacity (Figs. S10a-b).

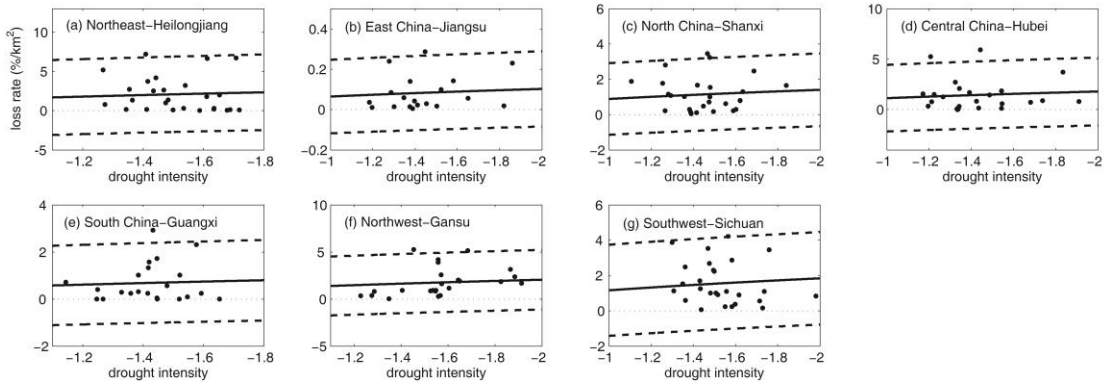

Fig. S8 Relationship between drought intensity by SPEI and economic losses per unit area for a representative province in seven sub-regions in China. Black dots denote recorded samples during the period 1984-2015 and the solid line is the fitting curve. Dashed lines are 95% uncertainty bounds. Multiple correlation coefficients of drought loss with drought intensity and exposed GDP in these provinces are between 0.7-0.89 (significant at 0.05 level).

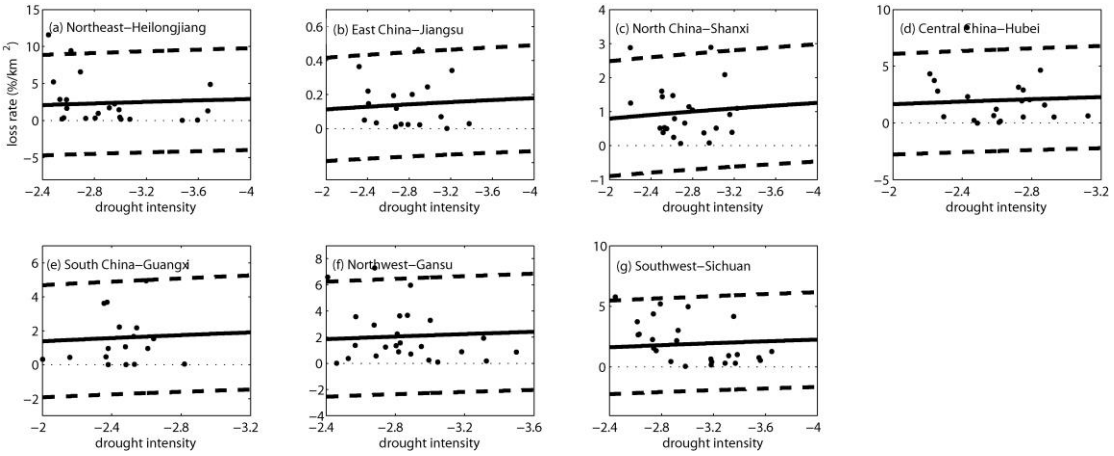

Fig. S9 Relationship between drought intensity by PDSI and economic losses per unit area for a representative province in seven sub-regions in China. Black dots denote recorded samples during the period 1984-2015 and the solid line is the fitting curve. Dashed lines are 95% uncertainty bounds. Multiple correlation coefficients of drought loss with drought intensity and exposed GDP in these provinces are 0.69-0.84 (significant at 0.05 level).

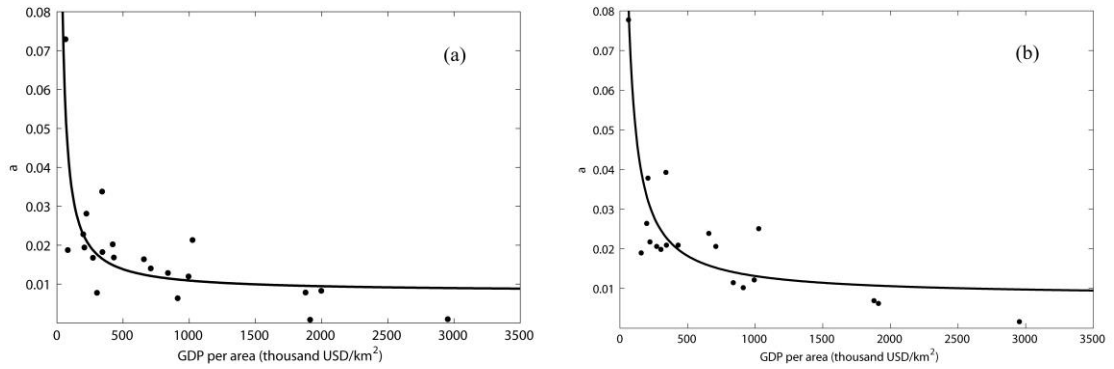

Fig. S10 Changes of variable *a* in the SPEI intensity-loss rate curve (a) and the PDSI intensity-loss rate curve (b) with GDP per unit area for 1984-2015 in China. Each black circle corresponds to one province, and the solid line is the fitting curve.

SI 8: Comparison of drought losses and their share of GDP in the warming world with the historical period

Table S6 illustrates annual drought losses and their share of GDP by median of twenty two model runs for several horizons: observational periods 1986-2005 and 2006-2015, future horizons for the 1.5 ºC warming under pathways SSP1 and SSP4, as well as the 2.0 ºC warming under pathways SSP2, SSP3 and SSP5. Meantime, annual growth of GDP under different SSPs is calculated for each

twenty years period to deduce share of drought losses to GDP growth.

Table S6 Mean annual drought losses and their share of GDP

Horizon	Loss (billion USD)		Loss/GDP (%)		GDP (billion USD)	Annual growth of GDP (billion USD)	Loss/Growth of GDP (%)	
1986-2005	4.2		0.23		1798 (734~3988)	163	2.6	
2006-2015	12.8		0.16		7950 (4603~11063)	646	2.0	
	SPEI	PDSI	SPEI	PDSI			SPEI	PDSI
1.5 ºC world under SSP1	46	48	0.19	0.19	24739 (16517~31985)	773	6.0	6.2
1.5 ºC world under SSP4	46	47	0.19	0.19	24597 (15976~31935)	798	5.8	5.9
2.0 ºC world under SSP2	78	67	0.21	0.18	36442 (32716~39391)	334	23.4	20.1
2.0 ºC world under SSP3	63	54	0.21	0.19	29105 (27189~29880)	135	46.7	40.0
2.0 ºC world under SSP5	88	77	0.21	0.19	41227 (34287~47415)	656	13.4	11.7

SI 9: Droughts by the SPI indices and estimated drought losses

According to SPI, drought intensity will increase from approximately -1.86 (severely dry) at the reference period to -2.00 (extremely dry) and -1.93 (severely dry) at the 1.5°C and the 2.0°C warming level, respectively. But decrease of drought area is projected with the warming of climate. The annual averaged drought area might decrease from approximately 482,500 km^2 to 430,800 km^2 and 399,500 km^2 at the 1.5°C and the 2.0°C warming, respectively. Frequency of drought events with different contiguous areas in China also shows a decreasing trend in the warming world (Fig. S11).

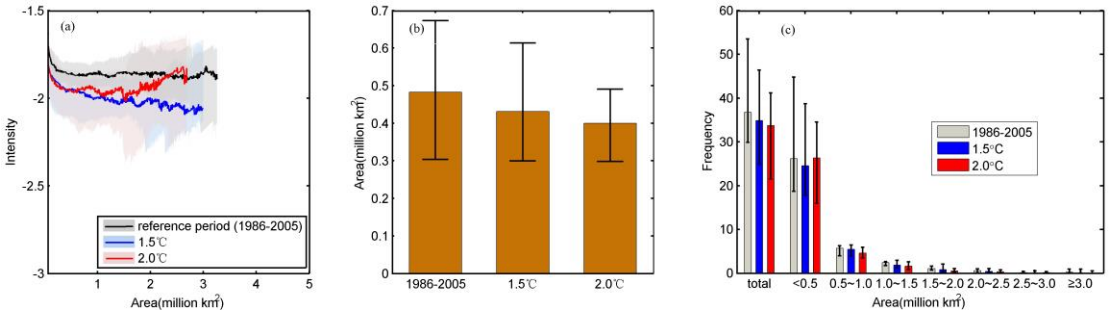

Fig. S11 Averaged drought intensity at different contiguous drought areas (a), averaged coverage of drought events (b) and annual frequency of drought events with different coverage (c) in China for the 1.5°C and 2.0°C global warming levels and the reference period (1986-2005). Shadows and lines in (a) are the bands and median, respectively, by twenty-two GCM runs. Histograms and black vertical lines in (b), and (c) denote the median and range of multi-model projections, respectively.

According to the "intensity-loss rate" curve with consideration of the adaption capacity (Fig. S12), drought losses by the SPI are estimated in the warming world. Follows the SSP1 and SSP4 to the 1.5 °C warming level, drought loss will reach about 33 billion USD by median with 95% confidence interval of 28-37, which is approximately 8 times of that in the reference period. Projected annual average loss accounts for 0.13% of the national GDP for the 1.5°C warming, lower than that of observational records. For the 2.0°C warming level, drought losses might be 39 [95% confidence interval: 35-45] billion USD, 32 [95% confidence interval: 29-37] billion USD, and 45 [95% confidence interval: 40-51] billion USD under the SSP2, SSP3 and SSP5, respectively. Projected annual average loss will further decrease to make up 0.11% of the projected national GDP (Fig. S13 and Table S7).

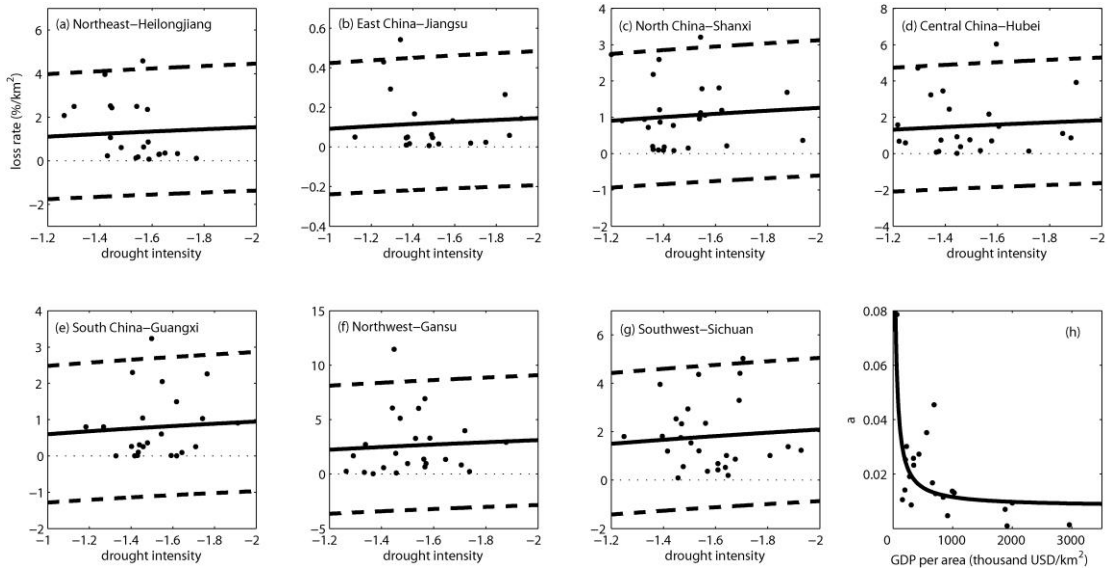

Fig. S12 Relationship between drought intensity by SPI and economic losses per unit area for a representative province in seven regions in China (a-g). Black dots denote recorded samples during the period 1984-2015 and the solid line is the fitting curve. Dashed lines are 95% uncertainty bounds. Multiple correlation coefficients of drought loss with drought intensity and exposed GDP in these provinces are 0.51-0.88 (significant at 0.05 level). Changes of variable *a* in the SPI intensity-loss rate curve with GDP per unit area for 1984-2015 in China is shown in (h). Each black circle corresponds to one province, and the solid line is the fitting curve.

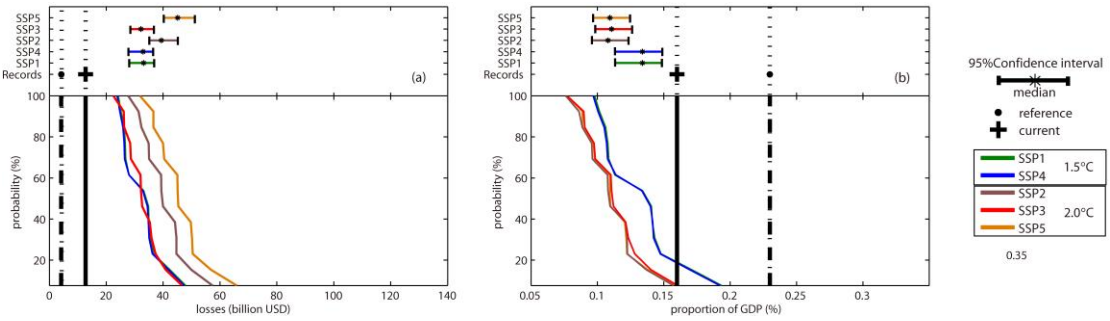

Fig. S13 Drought losses (a) and their share of GDP (b) at the 1.5°C and 2.0°C global warming levels under SSP1-5 development pathways in China. Probability in vertical axis represents percentage of

the total number exceeding a given loss or given share of GDP in twenty-two modeling results. Dotted black lines denote the recorded annual mean loss and its share of GDP in the reference period (1986-2005) and current status (2006-2015). 95% confidence intervals of projected losses and share of GDP are shown in the figure under different development pathways. Asterisk is the multi-model median.

Table S7 Mean annual drought losses and their share of GDP by SPI

	Loss (billion USD)	Loss/GDP (%)
1.5 ºC world under SSP1	33	0.13
1.5 ºC world under SSP4	33	0.13
2.0 ºC world under SSP2	39	0.11
2.0 ºC world under SSP3	32	0.11
2.0 ºC world under SSP5	45	0.11

SI 10: Droughts losses under constant GDP in 2010 under the warming scenarios

Effect of climate change on drought losses can be explored by the projected droughts under the warming climate and the constant GDP in 2010 (Table S6). Under the assumption of fixed GDP, drought losses will be 19 billion and 19.4 billion USD at the 1.5 ºC level, by the SPEI and PDSI, respectively, and will reach at 21.8 billion and 20.2 billion USD at the 2.0 ºC level. That is to say, warming climate will lead to a 48%-52% folds and 58%-70% folds higher drought losses in China under the 1.5 ºC and 2.0 ºC warming scenarios, respectively, than the recent interval of 2006-2015 (Table S8 and S6).

Table S8 Mean annual drought losses estimated under constant GDP in 2010

Warming Scenario	Loss（billion USD）		
	SPEI	PDSI	SPI
1.5 ºC	19.0	19.4	12.5
2.0 ºC	21.8.	20.2	11.1

References

1. Li H, Sheffield J, Wood EF (2010) Bias correction of monthly precipitation and temperature fields from Intergovernmental Panel on Climate Change AR4 models using equidistant quantile matching, *Journal of Geophysical. Research*.115, D10101
2. Wood AW, Leung LR, Sridhar V, Lettenmaier DP (2004) Hydrologic implications of dynamical and statistical approach to downscaling climate model outputs. *Climatic Change* 62(1-3): 189-216.
3. McKee TB, Doesken NJ, Kleist J (1993) The relationship of drought frequency and duration to time scales. Proceedings of the Eighth Conference on Applied Climatology, American Meteorological Society: Boston, 179-184.
4. Vicente-Serrano SM, Begueria S, Lopez-Moreno JI (2010) A multiscalar drought index sensitive

to global warming: the Standardized Precipitation Evapotranspiration Index. *Journal of Climate*, 23(7):1696-1718.
5. Palmer WC(1965) Meteorological drought, U.S. Weather Bureau Research Paper. 45, Washington, DC.
6. Wells N, Goddard S (2004) A Self-Calibrating Palmer Drought Severity Index. *Journal of Climate*17(12):2335-2351.
7. Allen RG, Pereira LS, Raes D, Smith M (1998) Crop evapotranspiration-guidelines for computing crop water requirements. FAO Irrigation and Drainage Paper 56, FAO, Rome.
8. Milly PCD and Dunne A (2017) A hydrologic drying bias in water-resource impact analyses of anthropogenic climate change. *Journal of the American Water Resources Association* 53(4): 822-838.
9. Milly PCD and Dunne A (2016) Potential evapotranspiration and continental drying. *Nature Climate Change* 6:946-950.
10. McAneney KJ and Itier B (1996) Operational limits to the Priestley-Taylor formula. *Irrigation Science* 17:37-43.
11. Tabari H, Talaee PH (2011) Local calibration of the Hargreaves and Priestley-Taylor equations for estimating reference evapotranspiration in arid and cold climates of Iran based on the Penman-Monteith model. *Journal of Hydrologic Engineering* 16:837-845.
12 Cristea NC, Kampf SK, Burges SJ (2012) Revised coefficients for the Priestley-Taylor and Makkikin-Hansen equations for estimating daily reference evapotranspiration. *Journal of Hydrologic Engineering* 18:1289-1300.
13. Didari S and Ahmadi SH (2018) Calibration and evaluation of the FAO56-Penman-monteith, FAO24-radiation, and Priestly-Taylor reference evapotranspiration models using the spatially measured solar radiation across a large arid and semi-arid area in southern Iran. *Theoretical and Applied Climatology* https://doi.org/10.1007/s00704-018-2497-2.
14. Oudin L, Hervieu F, Michel C, Perrin C, Andreassian V, Anctil F, Loumagne C (2005) Which potential evapotranspiration input for a lumped rainfall-runoff model?: Part 2- Towards a simple and efficient potential evapotranspiration model for rainfall-runoff modeling. *Journal of Hydrology* 303:290-306.
15. Hargreaves GH and Samani ZA (1985) Reference crop evapotranspiration from temperature. *Applied Engineering in Agriculture* 1(2):96-99.
16. Thornthwaite CW (1948) An approach toward a rational classification of climate. *Geographical Review* 38:55-94.
17. Hamon WR (1963) Computation of direct runoff amounts from storm rainfall. *International Association of Hydrological Sciences* 63:52-62.
18. Shuttleworh WJ (1993) Evaporation. In: Handbook of Hydrology, Maidment DR (editor). McGraw-Hill, New York, USA.
19. Priestley C and Taylor R (1972) On the assessment of surface heat flux and evaporation using large scale parameters. *Monthly Weather Review* 100:81-92.
20. Huang JL, Zhai JQ, Su BD, Wang YJ, Li XC, Jiang T, Fischer T (2017) Analysis of future drought characteristics in China using the regional climate model CCLM, *Climate Dynamics* 50(1-2):507-525.
21. Zhai, JQ, Huang JL, Su BD, Cao LG, Wang YJ, Jiang T, Fischer T (2017) Intensity-area-duration analysis of droughts in China 1960-2013. *Climate Dynamics* 48(1-2):151-168.

22. China Meteorological Administration (2016) Yearbook of Meteorological Disaster in China. China Meteorological Press, Beijing.
23. Wang AH, Lettenmaier DP, Sheffield J (2011) Soil moisture drought in China, 1950-2006. *Journal of Climate* 24(13):3257-3271.
24. Sheffield J, Wood EF, Roderick ML (2012) Little change in global drought over the past 60 years. *Nature* 491(7424): 435-438.
25. Collins M, Knutti R, Arblaster JM, Dufresne JL, Fichefet T, Friedlingstein P, Gao X., Gutowski WJ, Johns T, Krinner G, Shongwe M, Tebaldi C, Weaver AJ, Wehner M (2013) Long-term climate change: projections, comments and irreversibility. In: Climate Change 2013: The physical science basis. Contribution of working group I to the Fifth Assessment Report of the Intergovernmental Panel on Climate Change [Stocker T F, Qin D, Plattner G K, et al. (eds.)]. Cambridge University Press, Cambridge, United Kingdom and New York, NY, USA: 1029-1136.
26. Dellink R, Chateau J, Lanzi E, Magne B (2017) Long-term economic growth projections in the Shared Socioeconomic Pathways. *Global Environmental Change* 42: 200-214.